Chapter 3

STEERING CONTROL FOR AUTOMATED LANE KEEPING

Kinematic and dynamic models for lateral vehicle dynamics were discussed in the previous chapter. This chapter discusses lateral control systems used to control a vehicle to stay in the center of its lane.

The chapter is organized as follows. Control design by state feedback is discussed first in section 3.1. Steady state errors and the steady state steering angle required to negotiate a curved road are analyzed in sections 3.2 and 3.3. The subsequent sections of the chapter concentrate on control design by output feedback (sections 3.5, 3.6, 3.7, 3.8, 3.9 and 3.10).

3.1 STATE FEEDBACK

As seen in the previous chapter, under the small slip angle and bicycle model assumptions, the state space model for the lateral dynamics of the vehicle is given by

$$\dot{x} = Ax + B_1\delta + B_2\dot{\psi}_{des} \tag{3.1}$$

with $x = \{e_1 \quad \dot{e}_1 \quad e_2 \quad \dot{e}_2\}^T$, where e_1 is the lateral position error of the c.g., e_2 is the yaw angle difference between the vehicle and the road, δ is the front wheel steering angle input, $\dot{\psi}_{des}$ is the desired yaw rate determined by road curvature and vehicle speed and the matrices A, B_1 and B_2 have been presented earlier in Chapter 2 (section 2.5, equation (2.45)).

The following values of vehicle parameters will be used for all the simulations in this chapter.

R. Rajamani, *Vehicle Dynamics and Control*, Mechanical Engineering Series,
DOI 10.1007/978-1-4614-1433-9_3, © Rajesh Rajamani 2012

$m = 1573,\ I_z = 2873,\ \ell_f = 1.1,\ \ell_r = 1.58,\ C_{\alpha f} = 80000,\ C_{\alpha r} = 80000;$

These values are representative of parameters for a passenger sedan.

The open-loop matrix A has two eigenvalues at the origin and is unstable. The system has to be stabilized by feedback.

Calculations show that the pair (A, B_1) is controllable. Hence, using the state feedback law

$$\delta = -Kx = -k_1 e_1 - k_2 e_2 - k_3 e_3 - k_4 e_4 \tag{3.2}$$

the eigenvalues of the closed-loop matrix $(A - BK)$ can be placed at any desired locations. The closed-loop system using this state feedback controller is

$$\dot{x} = (A - B_1 K)x + B_2 \dot{\psi}_{des} \tag{3.3}$$

The following Matlab command can be used to place the eigenvalues of the closed-loop system.

K = place(A,B1,P)

This command yields a feedback matrix K such that the eigenvalues of the matrix $A - B_1 K$ are at the desired locations specified in the vector P.

Eigenvalues placed at $\begin{bmatrix} -5-3j & -5+3j & -7 & -10 \end{bmatrix}^T$ lead to the following simulation results shown in Figures 3-1, 3-2 and 3-3.

In these simulations a longitudinal speed of 30 m/s is used. The road is initially straight and then becomes circular with a radius of 1000 meters starting at a time of 1 second. The corresponding desired yaw rate can be calculated from $\dot{\psi}_{des} = \frac{V_x}{R} = 0.03 \text{ rad/s} = 1.72 \text{ deg/s}$. The desired yaw rate is shown in Figure 3-1 and is a step input from 0 to 1.72 deg/sec at 1 second. The time histories of the lateral error e_1 and yaw angle error e_2 are shown in Figure 3-2 and Figure 3-3 respectively.

Due to the presence of the $B_2 \dot{\psi}_{des}$ term in equation (3.3), the tracking errors need not all converge to zero, even though the matrix $(A - B_1 K)$ is stable. The steady state values of e_1 and e_2 are non-zero because the input due to road curvature $\dot{\psi}_{des}$ is non-zero. A physical interpretation of these steady state errors is provided in sections 3.2 and 3.3.

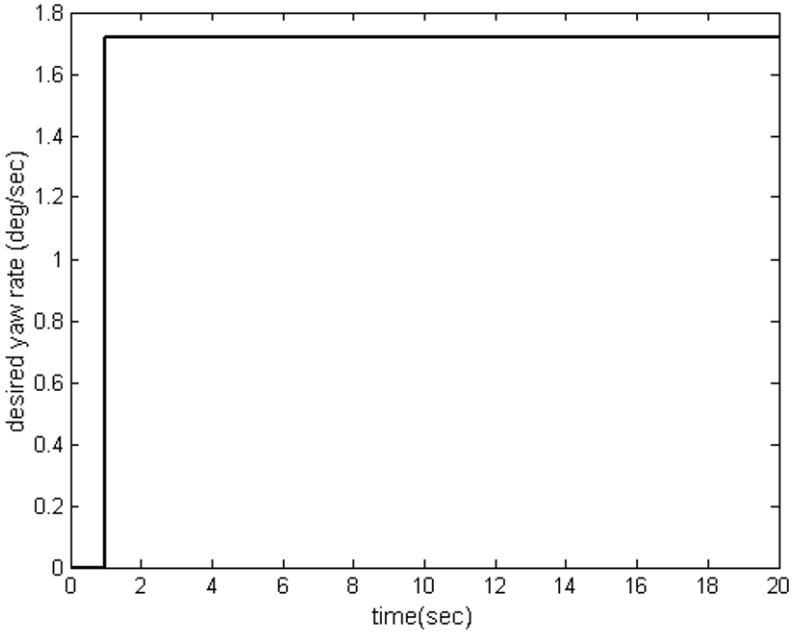

Figure 3-1. Desired yaw rate for simulations

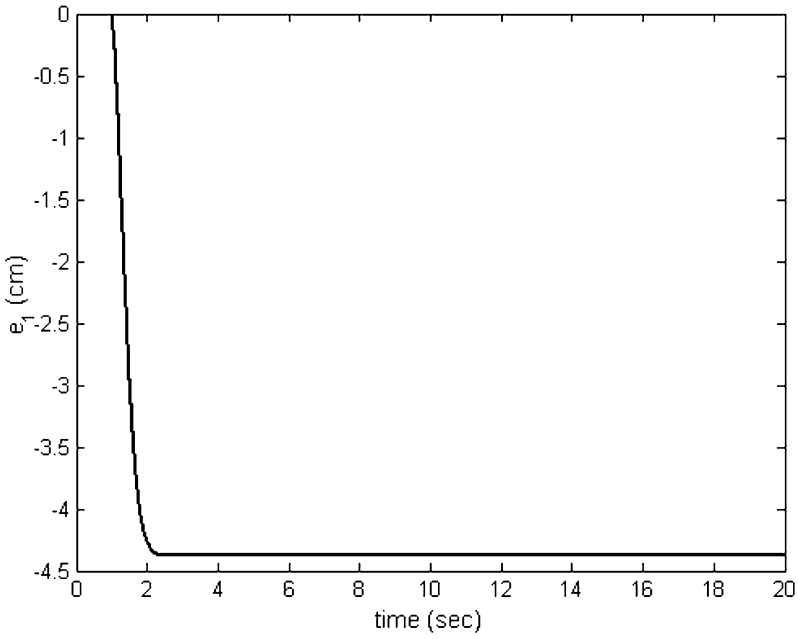

Figure 3-2. Lateral position error using state feedback

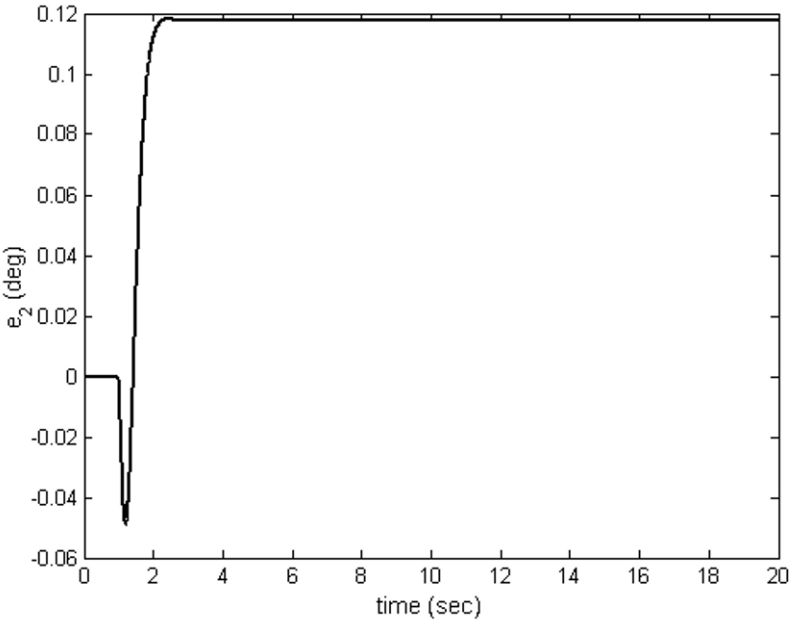

Figure 3-3. Yaw angle error using state feedback

3.2 STEADY STATE ERROR FROM DYNAMIC EQUATIONS

As before, the state space model for the closed-loop lateral system under state feedback is given by

$$\dot{x} = (A - B_1 K)x + B_2 \dot{\psi}_{des}$$

Due to the presence of the $B_2 \dot{\psi}_{des}$ term, the tracking errors will not all converge to zero when the vehicle is traveling on a curve, even though the matrix $(A - B_1 K)$ is asymptotically stable.

In this section, we will investigate whether the use of a feedforward term in addition to state feedback can ensure zero steady state errors on a curve. Assume that the steering controller is obtained by state feedback plus a feedforward term that attempts to compensate for the road curvature:

$$\delta = -Kx + \delta_{ff} \tag{3.4}$$

Then, the closed-loop system is given by

$$\dot{x} = (A - B_1 K)x + B_1 \delta_{ff} + B_2 \dot{\psi}_{des} \tag{3.5}$$

Taking Laplace transforms, assuming zero initial conditions, we find

$$X(s) = \left[sI - (A - B_1 K)\right]^{-1} \left\{B_1 L\left(\delta_{ff}\right) + B_2 L\left(\dot{\psi}_{des}\right)\right\} \tag{3.6}$$

where $L\left(\delta_{ff}\right)$ and $L\left(\dot{\psi}_{des}\right)$ are Laplace transforms of δ_{ff} and $\dot{\psi}_{des}$ respectively.

If the vehicle travels at constant speed V_x on a road with constant radius of curvature R, then

$$\dot{\psi}_{des} = \text{constant} = \frac{V_x}{R} \tag{3.7}$$

and its Laplace transform is $\frac{V_x}{Rs}$. Similarly, if the feedforward term is constant, then its Laplace transform is $\frac{\delta_{ff}}{s}$.

Using the Final Value Theorem, the steady state tracking error is given by

$$x_{ss} = \lim_{t\to\infty} x(t) = \lim_{s\to 0} sX(s) = -(A - B_1 K)^{-1} \left\{B_1 \delta_{ss} + B_2 \frac{V_x}{R}\right\} \tag{3.8}$$

Evaluation of equation (3.8) using the Symbolic Toolbox in Matlab yields the steady state errors

$$x_{ss} = \begin{Bmatrix} \frac{\delta_{ff}}{k_1} \\ 0 \\ 0 \\ 0 \end{Bmatrix} + \begin{Bmatrix} -\frac{1}{k_1}\frac{mV_x^2}{R(\ell_f + \ell_r)}\left[\frac{\ell_r}{2C_{\alpha f}} - \frac{\ell_f}{2C_{\alpha r}} + \frac{\ell_f}{2C_{\alpha r}}k_3\right] - \frac{1}{k_1 R}\left[\ell_f + \ell_r - \ell_r k_3\right] \\ 0 \\ \frac{1}{2RC_{\alpha r}(\ell_f + \ell_r)}\left[-2C_{\alpha r}\ell_f\ell_r - 2C_{\alpha r}\ell_r^2 + \ell_f m V_x^2\right] \\ 0 \end{Bmatrix} \tag{3.9}$$

From equation (3.9), we see that the lateral position error e_1 can be made zero by appropriate choice of δ_{ff}. However, δ_{ff} cannot influence the steady state yaw error, as seen from equation (3.9). The yaw angle error has a steady state term that cannot be corrected, no matter how the feedforward steering angle is chosen. The steady state yaw-angle error is

$$\begin{aligned} e_{2\_ss} &= \frac{1}{2RC_{\alpha r}(\ell_f + \ell_r)}\left[-2C_{\alpha r}\ell_f\ell_r - 2C_{\alpha r}\ell_r{}^2 + \ell_f m V_x{}^2\right] \\ &= -\frac{\ell_r}{R} + \frac{\ell_f}{2C_{\alpha r}\left(\ell_f + \ell_r\right)}\frac{mV_x{}^2}{R} \end{aligned} \tag{3.10}$$

The steady state lateral position error can be made zero if the feedforward steering angle is chosen as

$$\delta_{ff} = \frac{mV_x{}^2}{RL}\left[\frac{\ell_r}{2C_{\alpha f}} - \frac{\ell_f}{2C_{\alpha r}} + \frac{\ell_f}{2C_{\alpha r}}k_3\right] + \frac{L}{R} - \frac{\ell_r}{R}k_3 \tag{3.11}$$

which upon closer inspection is seen to be

$$\delta_{ff} = \frac{L}{R} + K_V a_y - k_3\left[\frac{\ell_r}{R} - \frac{\ell_f}{2C_{\alpha r}}\frac{mV_x{}^2}{R\ell}\right] \tag{3.12}$$

where $K_V = \frac{\ell_r m}{2C_{\alpha f}\left(\ell_f + \ell_r\right)} - \frac{\ell_f m}{2C_{\alpha r}\left(\ell_f + \ell_r\right)}$ is called the understeer gradient and $a_y = \frac{V_x{}^2}{R}$. If we denote $m_r = m\frac{\ell_f}{L}$ as the portion of the vehicle mass carried on the rear axle and $m_f = m\frac{\ell_r}{L}$ as the portion of the vehicle mass carried on the front axle, then $K_V = \frac{m_f}{2C_{\alpha f}} - \frac{m_r}{2C_{\alpha r}}$.

Hence

$$\delta_{ff} = \frac{L}{R} + K_V a_y + k_3 e_{2\_ss} \tag{3.13}$$

The steady state steering angle for zero lateral position error is given by

$$\delta_{ss} = \delta_{ff} - Kx_{ss} \text{ or}$$

$$\delta_{ss} = \delta_{ff} - k_3 e_{2ss} \text{ or}$$

$$\delta_{ss} = \frac{L}{R} + K_V a_y \tag{3.14}$$

Table 3-1. Summary of state feedback controller with feedforward

SUMMARY OF STATE FEEDBACK CONTROLLER WITH FEEDFORWARD		
Symbol	Nomenclature	Equation
e_{2_ss}	Steady-state yaw angle error	$e_{2\_ss} = -\frac{\ell_r}{R} + \frac{\ell_f}{2C_r\left(\ell_f + \ell_r\right)}\frac{mV_x^2}{R} = -\frac{\ell_r}{R} + \alpha_r$
δ_{ss}	Steady-state steering angle	$\delta_{ss} = \frac{L}{R} + K_V a_y$
δ_{ff}	Feedforward component of steering angle	$\delta_{ff} = \frac{L}{R} + K_V a_y - k_3 e_{2\_ss}$
α_f	Slip angle at front tires	$\alpha_f = \frac{m_f}{2C_{\alpha f}}\frac{V_x^2}{R}$
α_r	Slip angle at rear tires	$\alpha_r = \frac{m_r}{2C_{\alpha r}}\frac{V_x^2}{R}$
K_V	Understeer gradient	$K_V = \frac{m_f}{2C_{\alpha f}} - \frac{m_r}{2C_{\alpha r}}$

In conclusion, the lateral position error e_1 can be made zero at steady state by appropriate choice of the feedforward input δ_{ff}. However, the steady state yaw angle will be equal to $e_{2\_ss} = -\frac{\ell_r}{R} + \frac{\ell_f}{2C_{\alpha r}\left(\ell_f + \ell_r\right)}\frac{mV_x^{\,2}}{R}$ and cannot be changed by the feedforward steering input.

3.3 UNDERSTANDING STEADY STATE CORNERING

3.3.1 Steering angle for steady state cornering

This section uses geometric analysis to provide an answer to the question "What is the steady state steering angle required to negotiate a curve of radius R?" (Gillespie, 1992, Wong, 2001). As expected, the geometric analysis provides the same answer as the feedforward system analysis of the previous section. However, a better physical understanding of the lateral tire force requirements is obtained from the geometric analysis.

As discussed in the previous chapter, the slip angle at each wheel is the angle between the orientation of the wheel and the orientation of its velocity vector. Let the slip angle at the front wheel be denoted by α_f and that at the rear wheel be denoted by α_r, as shown in Figure 3-4. The instantaneous turn center O of the vehicle is the point at which the two lines perpendicular to the velocities of the two wheels meet.

Let $L = \ell_f + \ell_r$ be the wheelbase i.e. the distance between the centers of the front and rear wheels. Then, from the above figure, the angle subtended at the center of rotation is $\delta - \alpha_f + \alpha_r$. Under the assumption that the road radius is much larger than the wheelbase of the vehicle ($R >> L$) (so that chord length is approximately equal to arc length), we have

$$\delta - \alpha_f + \alpha_r \approx \frac{L}{R} \tag{3.15}$$

Hence the steady state steering angle is given by

$$\delta = \frac{L}{R} + \alpha_f - \alpha_r \tag{3.16}$$

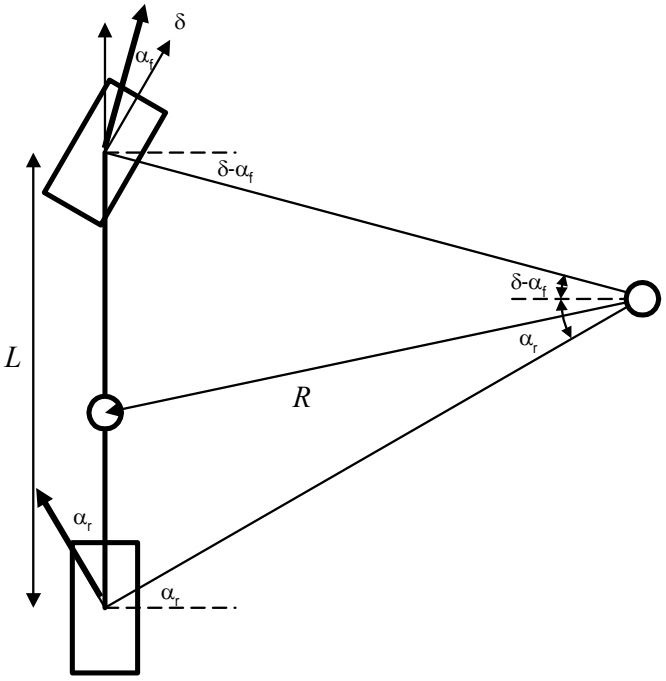

Figure 3-4. Steering angle for high speed cornering

The steady state slip angles α_f and α_r are related to the road radius as follows. Steady state force and moment equilibrium equations for the vehicle yield

$$F_{yf} + F_{yr} = m\frac{V_x^{\,2}}{R} \tag{3.17}$$

$$F_{yf}\ell_f - F_{yr}\ell_r = 0 \tag{3.18}$$

From the moment equilibrium (3.18) we have

$$F_{yf} = \frac{\ell_r}{\ell_f} F_{yr} \tag{3.19}$$

Using the relationship between front and rear tire forces of equation (3.19) in the force equilibrium equation (3.17), we have

$$F_{yr} = m\frac{\ell_f}{L}\frac{V_x^2}{R} = m_r\frac{V_x^2}{R} \tag{3.20}$$

where $m_r = m\dfrac{\ell_f}{L}$ is the portion of the vehicle mass carried on the rear axle. In words, the lateral force developed at the rear axle is m_r times the lateral acceleration. The same procedure can be used to find the front tire force :

$$F_{yf} = m\frac{\ell_r}{L}\frac{V_x^2}{R} = m_f\frac{V_x^2}{R} \tag{3.21}$$

where $m_f = m\dfrac{\ell_r}{L}$ is the portion of the vehicle mass carried on the front axle.

Assume that the slip angles are small so that the lateral tire force at each wheel is proportional to its slip angle. Denoting the cornering stiffness of each front tire by $C_{\alpha f}$ and that of each rear tire by $C_{\alpha r}$, and assuming that there are two front and two rear tires, the slip angles are

$$\alpha_f = \frac{F_{yf}}{2C_{\alpha f}} = \frac{m_f}{2C_{\alpha f}}\frac{V_x^2}{R},\ \alpha_r = \frac{F_{yr}}{2C_{\alpha r}} = \frac{m_r}{2C_{\alpha r}}\frac{V_x^2}{R} \tag{3.22}$$

The steady state steering angle is therefore given by

$$\delta = \frac{L}{R} + \alpha_f - \alpha_r = \frac{L}{R} + \left(\frac{m_f}{2C_{\alpha f}} - \frac{m_r}{2C_{\alpha r}}\right)\frac{V_x^2}{R}$$

or

$$\delta = \frac{L}{R} + K_V a_y \tag{3.23}$$

where the parameter K_V is called the understeer gradient and $a_y = \frac{V_x^2}{R}$. Equation (3.23) is the formula that relates vehicle velocity and road curvature to the steering angle required for negotiating the circular road. This is the same as equation (3.14) obtained previously.

Depending on the relative values of the front and rear cornering stiffness and mass distribution values, three possibilities exist for the value of K_V:

1. Neutral steer

In this case the understeer gradient K_V is zero due to equal slip angles at the rear and front tires.

$$\frac{m_f}{C_f} = \frac{m_r}{C_r} \Rightarrow K_V = 0 \Rightarrow \alpha_f = \alpha_r$$

In the case of neutral steer, on a constant radius turn, no change in the steering angle is required as speed is varied. The steering angle depends only on the curve radius and the wheelbase.

2. Understeer

In this case the understeer gradient $K_V > 0$ due to a larger slip angle at the front tires compared to the rear tires.

$$\frac{m_f}{C_f} > \frac{m_r}{C_r} \Rightarrow K_V > 0 \Rightarrow \alpha_f > \alpha_r$$

In the case of understeer, on a constant radius turn, the steering angle will have to increase with speed in proportion to K_V times the lateral acceleration.

3. Oversteer

In this case the understeer gradient $K_V < 0$ due to a smaller slip angle at the front tires compared to the rear tires.

$$\frac{m_f}{C_f} < \frac{m_r}{C_r} \Rightarrow K_V < 0 \Rightarrow \alpha_f < \alpha_r$$

In the case of oversteer, on a constant radius turn, the steer angle will have to decrease as the speed is increased.

The steering angle as a function of vehicle longitudinal speed is shown in Figure 3-5 for the three cases of neutral steer, understeer and oversteer. Note that in the case of oversteer, the steering angle decreases with speed and could eventually reach zero at a speed called critical speed.

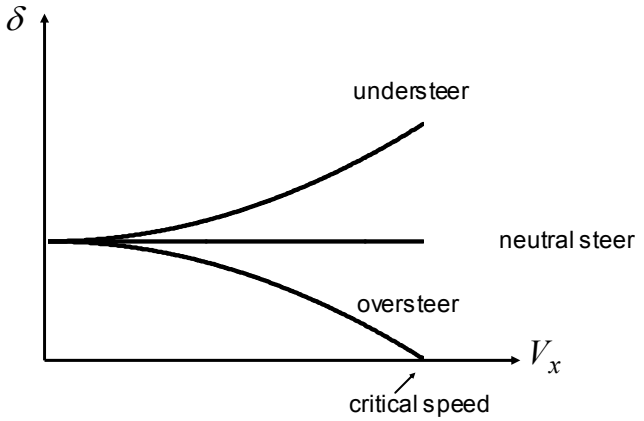

Figure 3-5. Steering angle variation with speed

3.3.2 Can the yaw-angle error be zero ?

If the parameters of the vehicle and the vehicle speed were such that

$$\frac{\ell_r}{R} = \frac{\ell_f}{2C_r\ell}\frac{mV_x^2}{R} \tag{3.24}$$

then the steady state yaw error of equation (3.10) would also be zero. This happens at one particular speed V_x at which equation (3.24) is satisfied and this speed is independent of the radius of the path.

The physical interpretation of equation (3.24) is as follows. The right hand side of the equation, as we have seen during the geometric analysis, is the slip angle at the rear tire. The left hand side of the equation is the angle γ subtended by the rear portion of the vehicle at the center of the circular path, as shown in Figure 3-6 below.

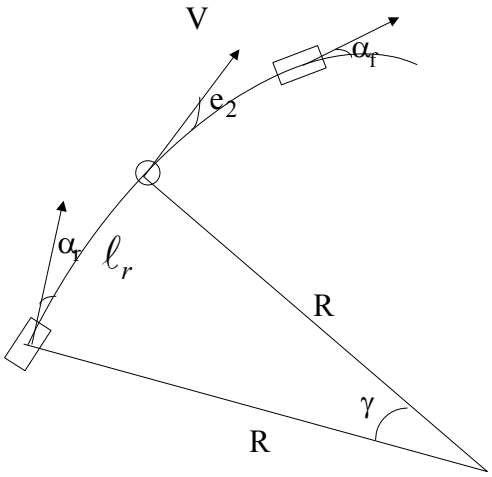

Figure 3-6. Steady state yaw angle error

Since the vehicle has a finite length, both its lateral position error and its yaw-angle error cannot always be made simultaneously zero. If the steady-state lateral position error is zero, then the steady state yaw-angle error can be zero only if the slip angle at the rear is the same as the angle γ subtended by the vehicle at the center of the circular path. This happens at one particular speed V_x at which equation (3.24) is satisfied and this speed is independent of the radius of the path.

3.3.3 Is non-zero yaw angle error a concern?

The above geometric analysis shows that no matter which control law is used, the yaw angle error e_2 will have a steady state value. This is because the slip angles at the rear and front wheels are completely determined, once the radius of the road and the vehicle speed V_x are fixed. Hence the slip angle of the vehicle β is automatically determined. The slip angle of the vehicle is

$$\beta = \frac{\dot{y}}{V_x} = \frac{1}{V_x}\left(\dot{e}_1 - V_x e_2\right) \tag{3.25}$$

Since the steady state value of $\dot{e}_1$ is zero, it follows that the steady state value of the vehicle slip angle is

$$\beta = -e_{2\_ss} \tag{3.26}$$

or

$$\beta = -(\psi - \psi_{des})_{ss}$$

Hence

$$(\beta + \psi)_{ss} = \psi_{des} \tag{3.27}$$

The steady state error in e_2 is not a cause of concern. We don't necessarily need e_2 to converge to zero – all we need is that the heading angle $\psi + \beta$ converge to the desired angle ψ_{des}. Since the steady state error in e_2 is equal to β, from equation (3.27), it is guaranteed that $\psi + \beta$ will converge to ψ_{des}.

3.4 CONSIDERATION OF VARYING LONGITUDINAL VELOCITY

In general the longitudinal vehicle speed can vary in which case the system matrices $A(V_x)$ and $B_1(V_x)$ are time varying (or parameter varying). A constant state feedback matrix K can be used to obtain stability for varying velocity by exploiting the convex nature of the lateral dynamic system. The approach is to choose K such that $A(V_x) - B_1(V_x)K$ is simultaneously quadratically stabilized at the two extreme values of V_x. The following Theorem summarizes the design result that can be used for full state feedback control system design.

Theorem 3.1:

Let the closed-loop matrix be defined as

$$A_{CL}(V_x) = A(V_x) - B_1(V_x)K \tag{3.28}$$

Let

$$A_{\min} = A_{CL}(V_{\min}) = A(V_{\min}) - B_1(V_{\min})K \text{ and}$$

$$A_{\max} = A_{CL}(V_{\max}) = A(V_{\max}) - B_1(V_{\max})K$$

be defined as the values of $A_{CL}(V_x)$ at the extremes of the varying parameter V_x.

If a constant state feedback matrix K is chosen such that

$$A_{\min}{}^T P + PA_{\min} < 0 \tag{3.29}$$

and

$$A_{\max}{}^T P + PA_{\max} < 0 \tag{3.30}$$

for some $P > 0$, then the closed-loop system is stable for velocity varying in the range $V_{\min} \le V_x \le V_{\max}$.

Proof:

First, note that the closed-loop matrix can be rewritten as a convex combination of $A_{\min}$ and $A_{\max}$:

$$A_{CL}(V_x) = A(V_x) - B_1(V_x)K = aA_{\min} + (1-a)A_{\max} \quad \text{with} \quad 0 \le a(V_x) \le 1 \tag{3.31}$$

where $a(V_x)$ is a parameter whose value depends on the operating speed V_x.

Using the Lyapunov function candidate $V = x^T Px$, we find that its derivative is

$$\dot{V} = \dot{x}^T Px + x^T P\dot{x} = x^T (A_{CL}{}^T P + PA_{CL})x$$

$$= ax^T (A_{\min}{}^T P + PA_{\min})x + (1-a)x^T (A_{\max}{}^T P + PA_{\max})x$$

$$< 0$$

Hence the proof.

3.5 OUTPUT FEEDBACK

The lateral position of the vehicle with respect to the road is usually measured at a location ahead of the vehicle, as shown in Figure 3-7. Sensor systems used for measurement of lateral position include differential GPS (Donath, et. al., 1997), vision cameras (Taylor, et. al., 1999, Thorpe, et. al., 1998) and magnetometers that measure the magnetic field from permanent magnets embedded in the roadway (Guldner, et. al., 1996).

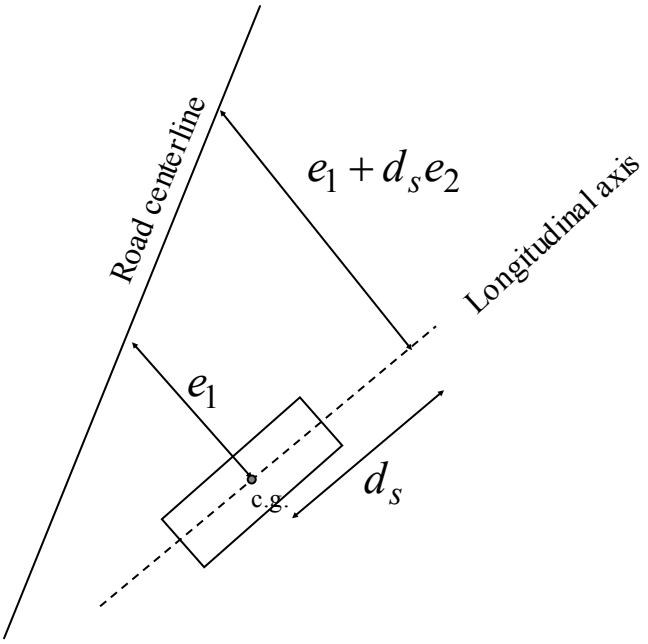

Figure 3-7. Look ahead lateral position measurement with respect to road

If we assume that the yaw angle error e_2 is small so that chord lengths can be approximated by arc lengths, then the measurement equation that relates the output to the states is as follows:

$$y = e_1 + d_s e_2 \tag{3.32}$$

where d_s is the longitudinal distance of the point ahead of the vehicle c.g. at which the sensor measurement is made.

3.6 UNITY FEEDBACK LOOP SYSTEM

Consider the following block diagram for the output feedback system shown in Figure 3-8. Here $P(s)$ is the plant transfer function between the steering angle input for the vehicle and the lateral position measurement output described in section 3.5. $C(s)$ represents the transfer function for the controller (to be determined later). The road-determined desired yaw rate $\dot{\psi}_{des}$ affects the system dynamics through a transfer function denoted in Figure 3-8 as $G(s)$. The signal $n(t)$ is the sensor noise that affects the system.

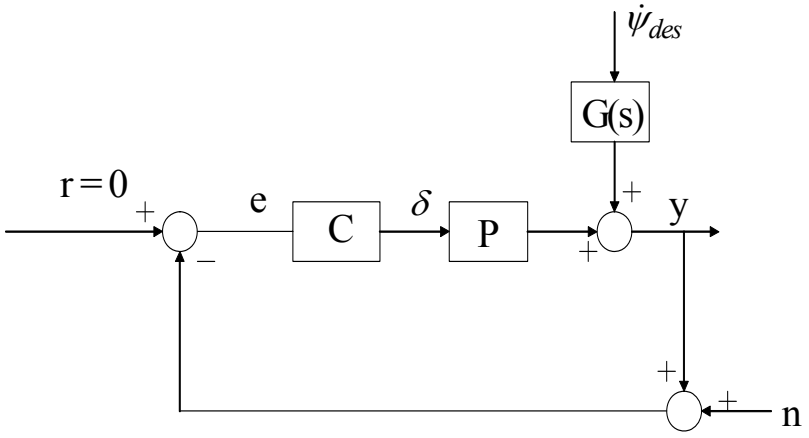

Figure 3-8. Unity feedback loop system

Figure 3-9 and Figure 3-10 shows the zeros and poles of $P(s)$ for values of d_s = 2.0 meters and d_s = 7.0 meters respectively. $P(s)$ has two poles at the origin, a pair of complex conjugate poles and a pair of complex conjugate zeros. Note that the zeros in Figure 3-10 are much better damped than the zeros in Figure 3-9. As d_s is increased, the damping increases for the complex conjugate pair of zeros. Figure 3-11 shows the magnitude and phase Bode plots for the plant transfer function $P(s)$ with d_s = 2 meters. A longitudinal velocity of 25m/s has been used in the model.

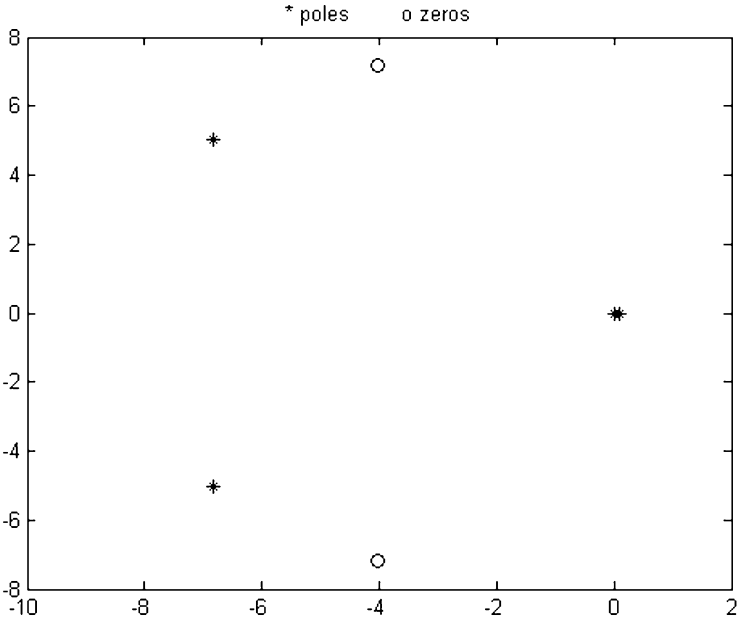

Figure 3-9. Zeros and poles of the open loop system for d_s = 2 meters

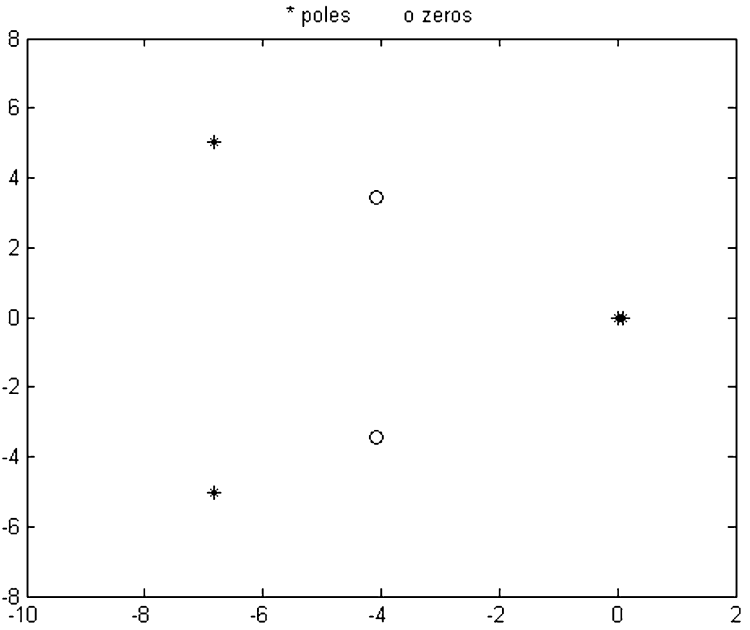

Figure 3-10. Zeros and poles of the open loop system for d_s = 7 meters

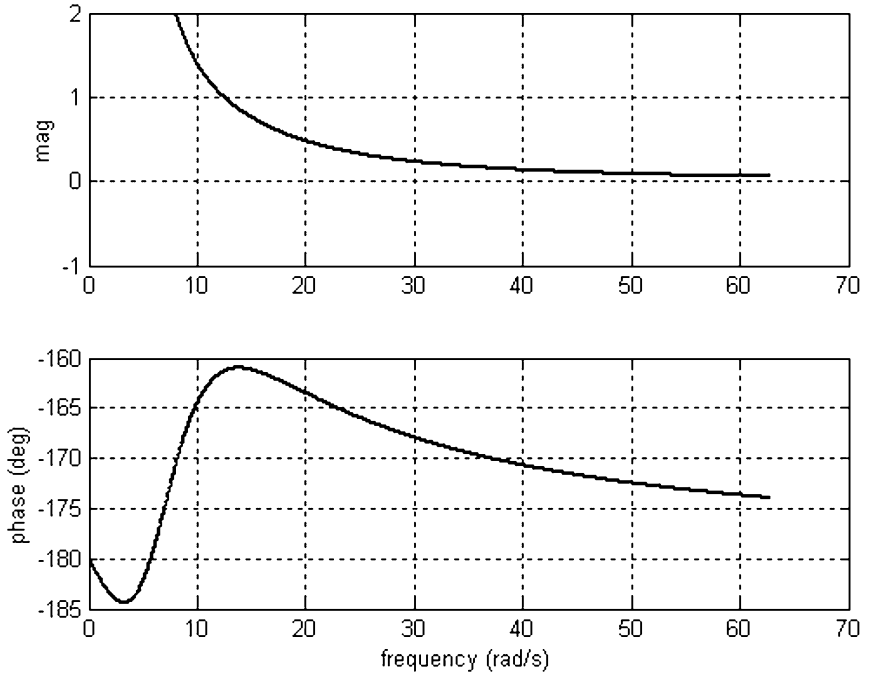

Figure 3-11. Bode plots for open-loop plant $P(s)$

3.7 LOOP ANALYSIS WITH A PROPORTIONAL CONTROLLER

An operating speed of 25 m/s and a sensor measurement location of $d_s = 2$ meters is assumed in this section for the lateral vehicle system. The open-loop transfer function $P(s)$ has two poles at the origin, an additional pair of complex conjugate poles and a pair of complex conjugate zeros. If the feedback loop were closed with a proportional controller, then $C(s) = K$ where K is the gain of the controller. The transfer function $PC(s)$ is of the type

$$PC(s) = \frac{\left(s^2 + 2\xi_n \omega_n s + {\omega_n}^2\right)}{s^2\left(s^2 + 2\xi_d \omega_d s + {\omega_d}^2\right)} \tag{3.33}$$

The contour Γ_s that s traverses in the complex plane for purposes of plotting the Nyquist plot must not pass through any poles or zeros of the open loop transfer function $PC(s)$. Hence it must not pass through the origin. Hence the following contour Γ_s as shown below in Figure 3-12 was used for the Nyquist plot. A semi-circle of radius ε is used to make a detour, so as to avoid going through the origin. By letting $\varepsilon \to 0$, the contour Γ_s will enclose the entire open right half plane.

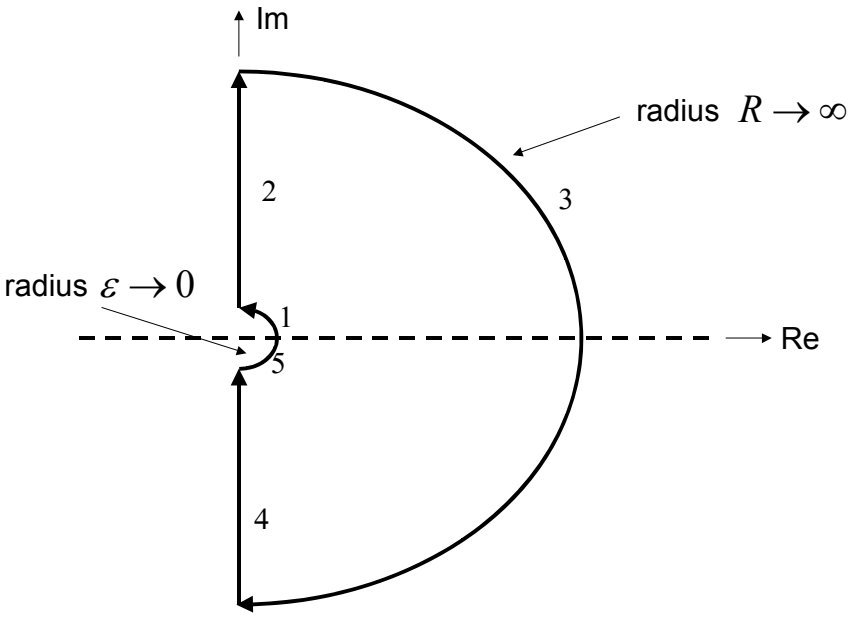

Figure 3-12. The Γ_s contour used for the Nyquist plot

Portions of the Γ_s contour have been marked as sections 1, 2, 3, 4 and 5. Section 3 consists of a semi-circle of radius R with $R \to \infty$ so as to cover the entire right half plane. The contour Γ_{PC} must be drawn for all values of s that s takes from the Γ_s contour. Section 3 of Γ_s gets mapped to the origin in the Γ_{PC} plane. It is important to draw the Γ_{PC} contour for sections 1, 2, 4 and 5 of Γ_s (see Figure 3-13) and determine how many times this contour encircles the –1 point. The Γ_{PC} contour for sections 1 and 2 is shown in the Nyquist plot in Figure 3-14.

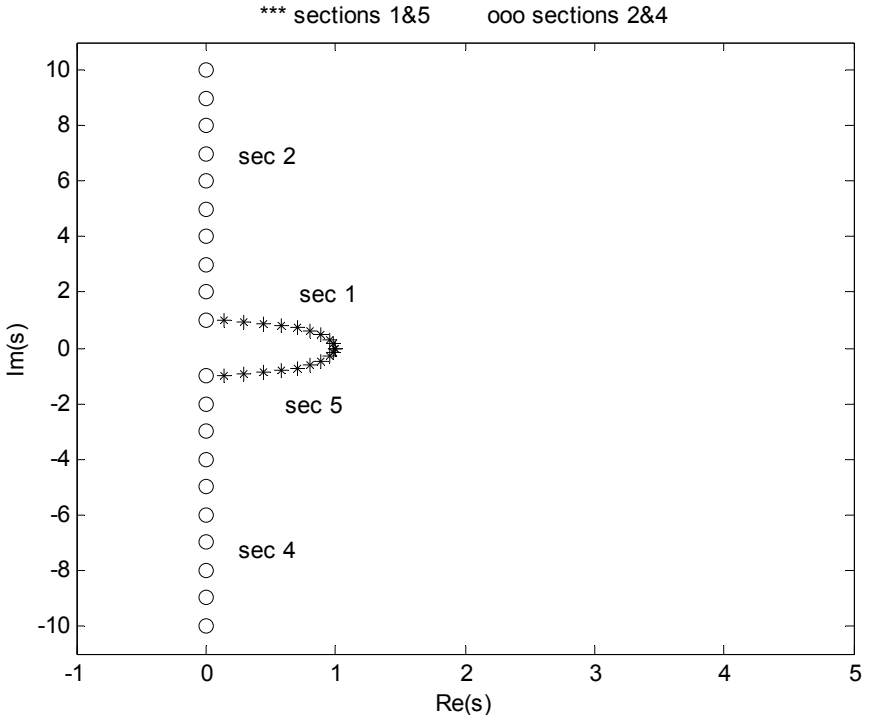

Figure 3-13. Sections 1, 2, 4 and 5 of the Γ_s contour used for the Nyquist plot

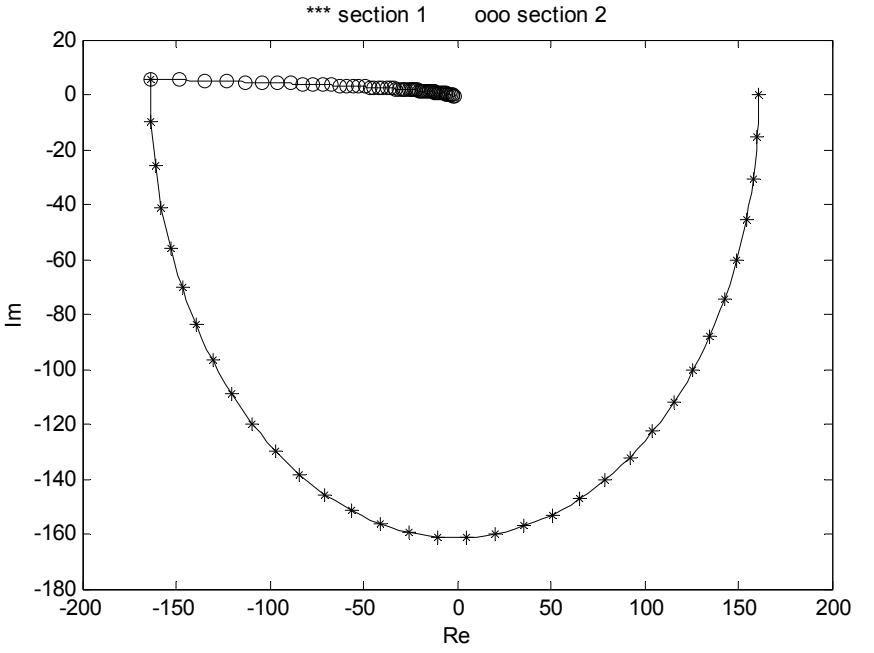

Figure 3-14. Nyquist plot (Γ_{PC} contour) obtained using sections 1 and 2 of the Γ_s contour

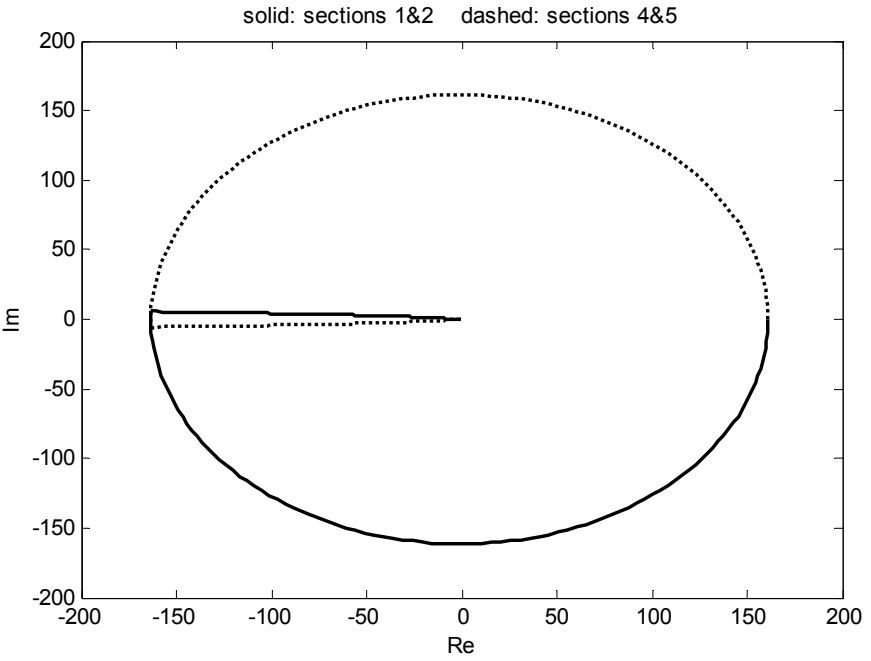

Figure 3-15. Nyquist plot obtained using sections 1, 2, 4 and 5 of the Γ_s contour

The Γ_{PC} contour corresponding to the entire Γ_s contour (sections 1, 2, 4 and 5) is shown in Figure 3-15. The solid line in this figure corresponds to sections 1 and 2 of Γ_s while the dashed line corresponds to sections 4 and 5 of Γ_s.

To determine how many times the above Γ_{PC} contour encircles the –1 point, it is necessary to zoom into the region near the –1 point, as is being done in Figure 3-16 and Figure 3-17. In Figure 3-16, a proportional gain of $K = 1$ is used. In this case, the Γ_{PC} contour encircles the –1 point twice: once clockwise and once counterclockwise. The clockwise encirclement can be easily seen in the big picture Nyquist plot of Figure 3-15. In the zoomed section of Figure 3-16, a counter clockwise encirclement can be seen. In the zoomed section of Figure 3-17, where the proportional gain is much smaller ($K = 0.01$), there is no counterclockwise encircelement of the –1 point. Thus in the case of the larger proportional gain, the total number of encircelements is $N = 1 - 1 = 0$ while in the case of the smaller proportional gain, the total number of encircelements is $N = 1$.

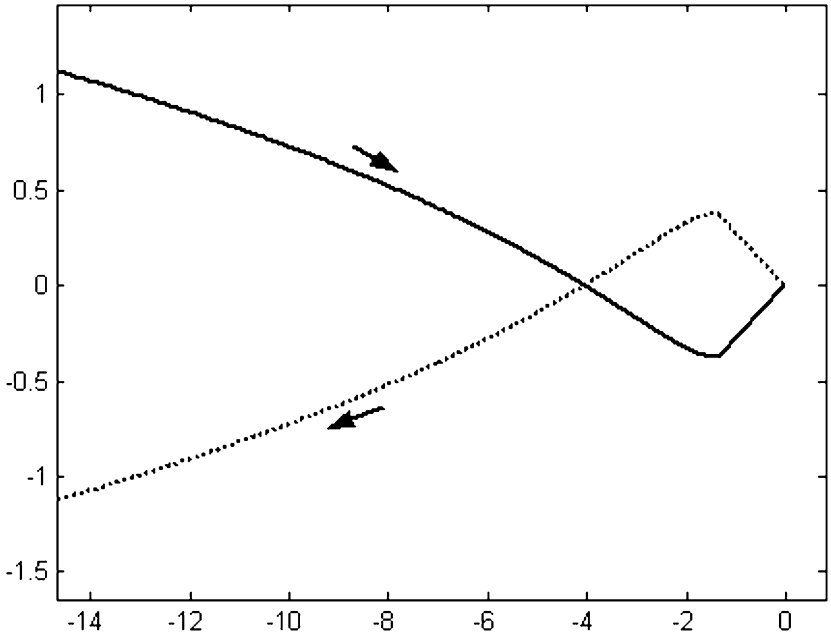

Figure 3-16. Zooming into the Nyquist plot: Gain = 1

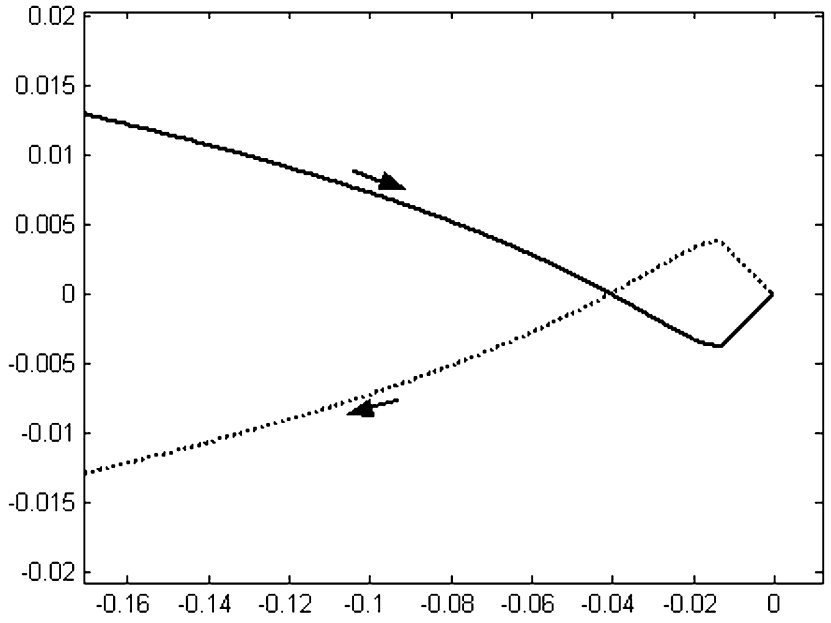

Figure 3-17. Zooming into the Nyquist plot: Gain = 0.01

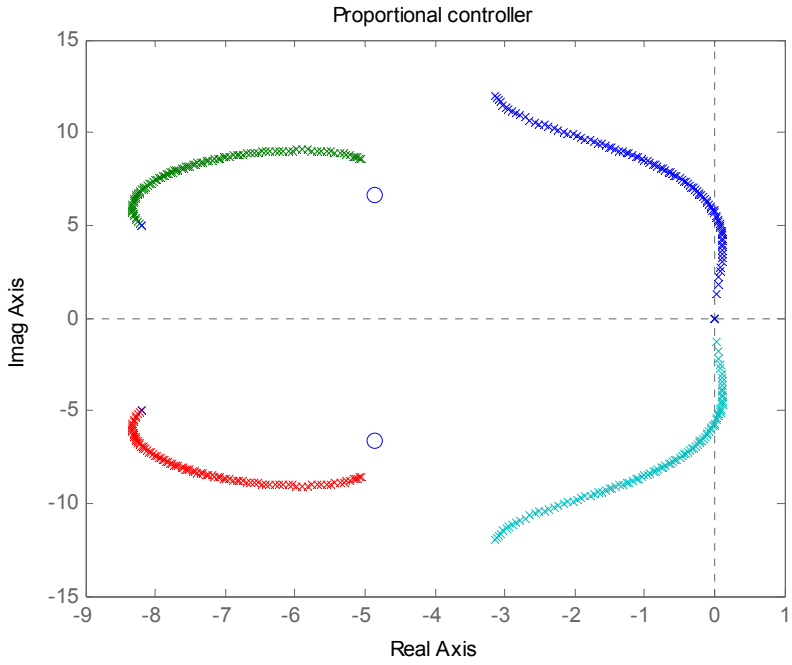

Figure 3-18. Root Locus with proportional controller

Thus the closed-loop system will be stable with proportional control if adequately large gain is used, but is unstable for small gain.

Figure 3-18 shows the root locus plot for varying feedback gain with the proportional controller. Again it can be seen that for small proportional gain, there is a pair of complex conjugate poles that are unstable. As the proportional gain is increased, these poles become stable.

It is important to note that with adequately large proportional gain, although the closed loop system gets stabilized, it still has poor phase margin. This can be seen from the Nyquist plots as well as the Bode plot showing the gain and phase margins in Figure 3-19. In Figure 3-19, with a proportional gain of 1, a phase margin of 18 degrees is obtained. It can be deduced from the plot that this is close to the best phase margin that can be obtained for this system. With a smaller gain of 0.1, the closed-loop system is unstable. With a higher proportional gain of 10, the system only has a phase margin of 8 degrees. Phase uncertainty can therefore easily change the number of encirclements of the –1 point for this system.

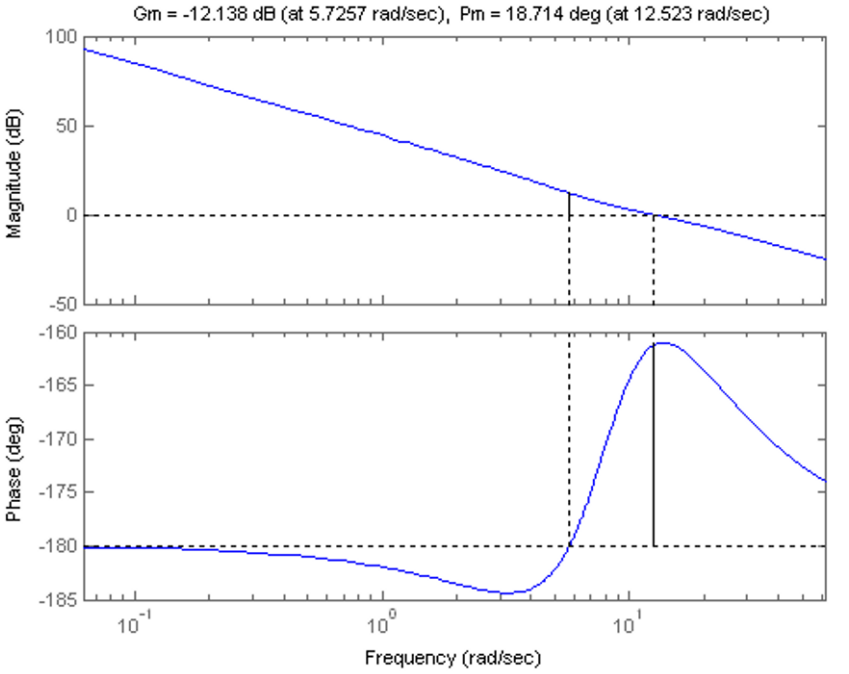

Figure 3-19. Gain margin and phase margin with a unity gain proportional controller

3.8 LOOP ANALYSIS WITH A LEAD COMPENSATOR

It is clear that robust gain and phase margin can be obtained if phase is added in the low frequency range (gain crossover range) for the system with unity feedback. Hence a lead compensator is suggested. The following transfer function can be used for the controller (compensator)

$$C(s) = K\frac{T_n s + 1}{T_d s + 1} \tag{3.34}$$

Values for T_n and T_d can be chosen so as to design the closed-loop system to have any desired value of phase margin. Values of $T_n = 0.5$ and $T_d = 0.1$ and $K = 0.01$ are used here as an illustration. In the plots shown in the next few pages, the above arbitrary values of T_n and T_d are used just to show that this compensator will increase the phase margin of the system.

Figure 3-20 shows the Bode plot for $PC(s)$ using the above lead compensator. Figure 3-23 shows the gain and phase margins of this system with a compensator gain $K = 1$. Figure 3-24 shows the gain and phase margins of this system with a compensator gain $K = 0.1$. It is clear that with the lead compensator phase has been added at the low frequencies to improve phase margin.

Figures 3-21 and 3-22 show the Nyquist plot for $PC(s)$. Figure 3-21 shows the Nyquist plot corresponding to sections 1 and 2 of Γ_s while Figure 3-22 shows the Nyquist plot corresponding to sections 1, 2, 4 and 5 of Γ_s. It is clear that the Nyquist curve does not encircle the –1 point and the closed-loop system is stable for all values of the compensator gain K.

Figure 3-25 shows the root locus plot for the system with lead compensator. Again, it is clear that the closed-loop system is stable for all values of the compensator gain K.

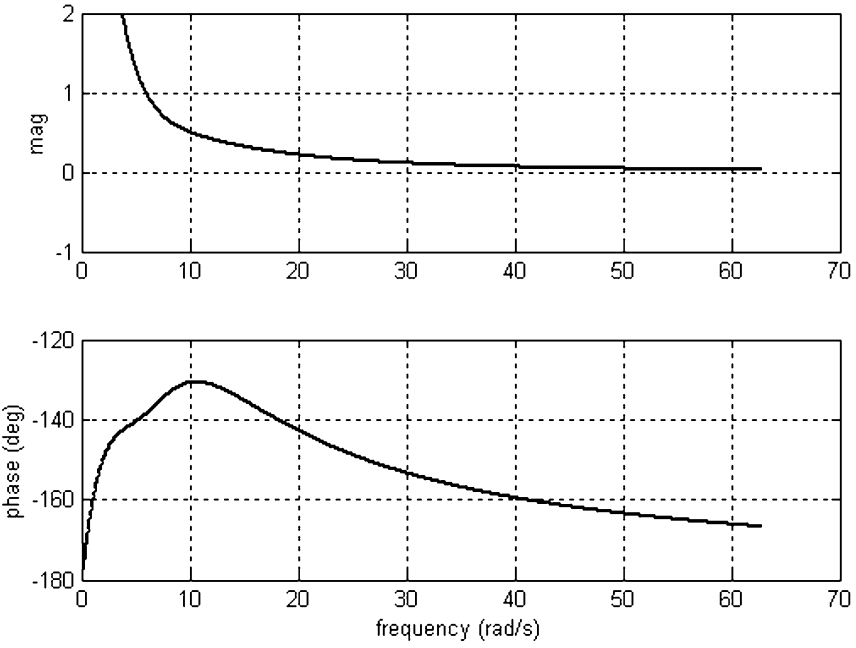

Figure 3-20. Bode plot for $PC(s)$ using a lead compensator (K = 0.01)

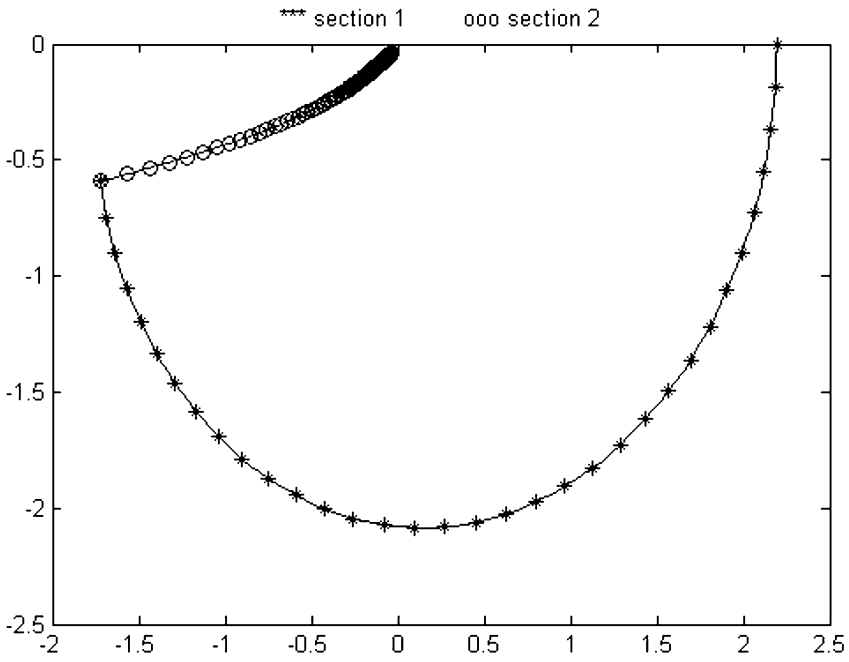

Figure 3-21. Nyquist plot corresponding to sections 1 and 2 of Γ_S (with lead compensator)

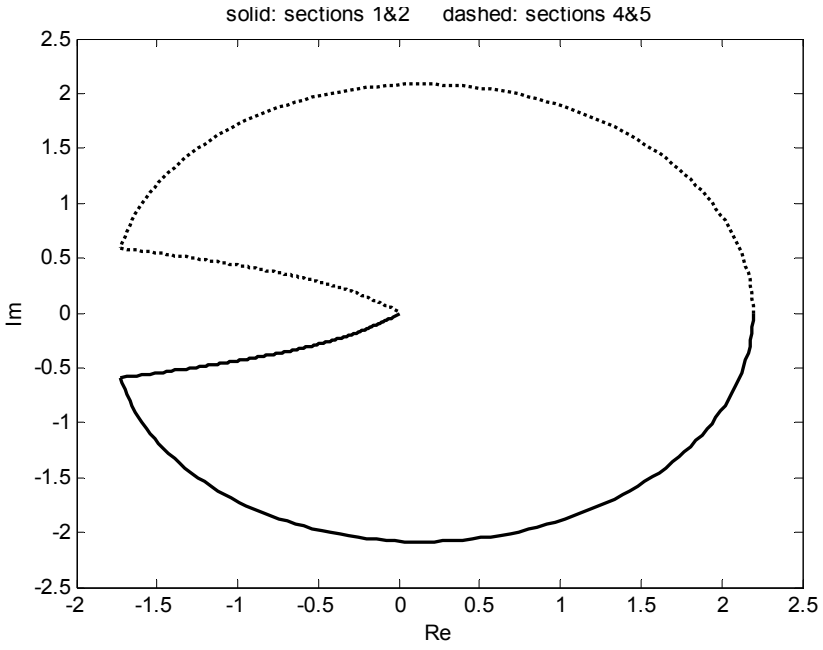

Figure 3-22. Nyquist plot corresponding to sections 1, 2, 4 and 5 of Γ_S (with lead compensator)

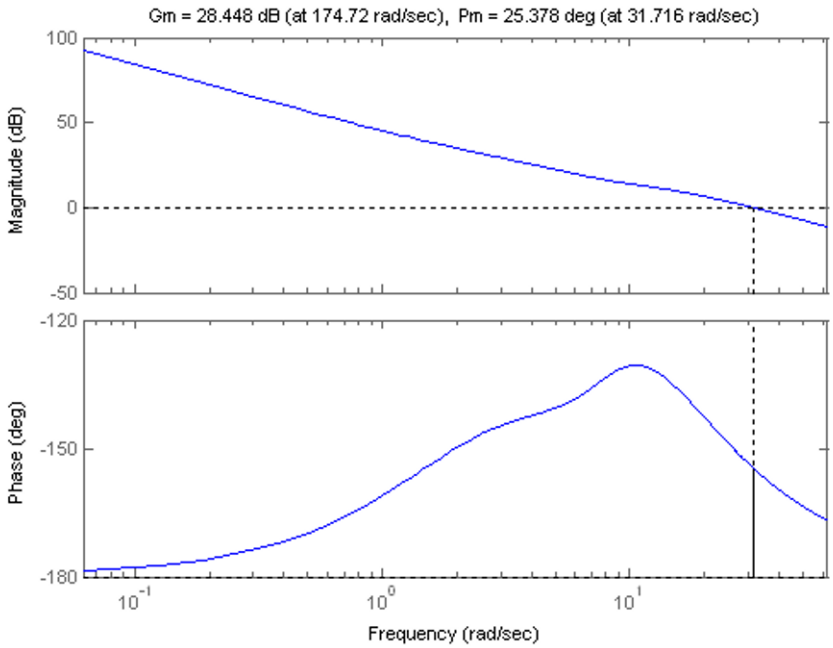

Figure 3-23. Bode plot showing gain and phase margins (with lead compensator, $K = 1$)

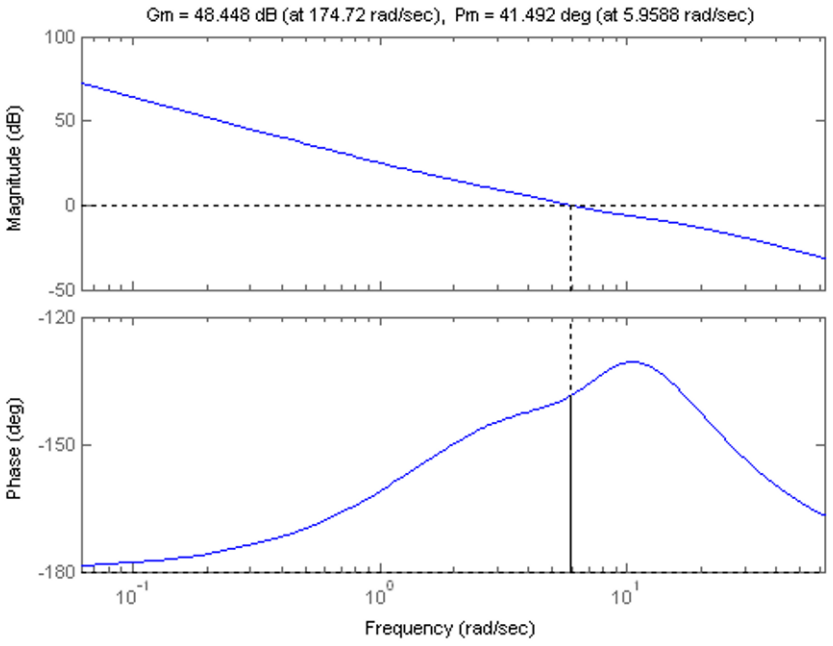

Figure 3-24. Bode plot showing gain and phase margins (with lead compensator, $K = 0.1$)

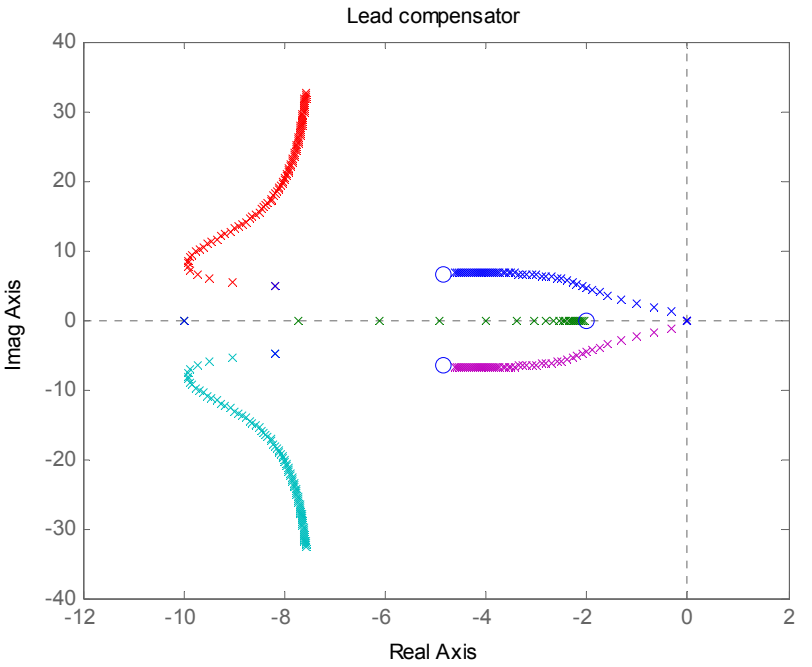

Figure 3-25. Root locus with lead compensator

3.9 SIMULATION OF PERFORMANCE WITH LEAD COMPENSATOR

To simulate the closed-loop system incorporating the lead compensator, the following state space extension can be used. The steering input is related to the sensor measurement by the following transfer function relation:

$$\delta(s) = -K\frac{T_n s + 1}{T_d s + 1} Y(s) \tag{3.35}$$

Hence, in the time domain,

$$T_d \dot{\delta} + \delta = -KT_n \dot{y} - Ky \tag{3.36}$$

Now

$$y = Cx$$

and

$$\dot{y} = CAx + CB_1\delta + CB_2\dot{\psi}_d$$

Since $CB_1 = 0$, $CB_2 = 0$, we have

$$T_d\dot{\delta} + \delta = -KT_nCAx - KCx \tag{3.37}$$

To find a state space model for the complete system including the lead compensator, define a fifth state

$$x_5 = \delta$$

Then, combining equation (3.37) and the previous linear time invariant model for the lateral system, the following extended state space representation can be used to represent the closed-loop dynamics:

$$\begin{bmatrix} \dot{x} \\ \dot{\delta} \end{bmatrix} = \begin{bmatrix} A & B_1 \\ -\frac{T_n}{T_d}KCA - \frac{1}{T_d}KC & -\frac{1}{T_d} \end{bmatrix} \begin{bmatrix} x \\ \delta \end{bmatrix} + \begin{bmatrix} B_2 \\ 0 \end{bmatrix} \dot{\psi}_d \tag{3.38}$$

3.10 ANALYSIS OF CLOSED-LOOP PERFORMANCE

3.10.1 Performance variation with vehicle speed

Bode plots of the transfer function of the open loop system from steering angle to yaw rate are shown in Figure 3-26 for various speeds. Speeds of 10, 20 and 30 m/s are shown, with the solid line representing 10 m/s, the dashed line respresenting 20 m/s and the solid line marked by '+'s representing 30 m/s. The plots show that the transfer function has less damping at higher speeds.

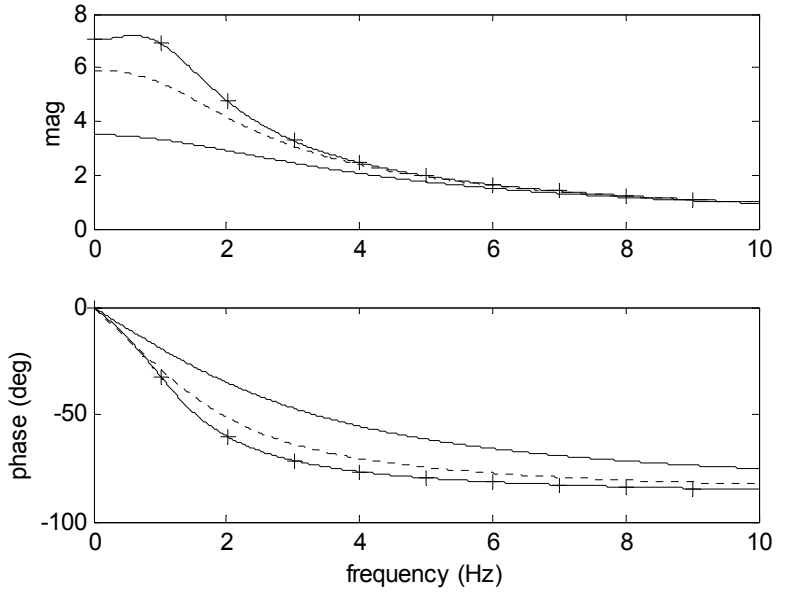

Figure 3-26. Transfer function from steering angle to yaw rate at various speeds

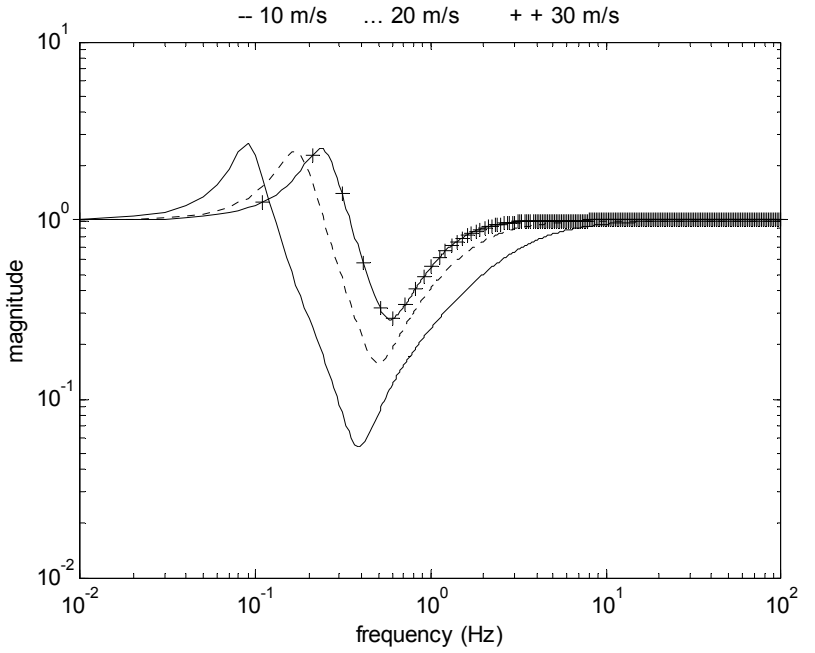

Figure 3-27. Closed-loop transfer function $\dot{\psi} / \dot{\psi}_{des}$ at different speeds (magnitude)

Using the same lead compensator discussed in section 3.7, Bode plots of the closed-loop transfer function $\frac{\dot{\psi}}{\dot{\psi}_d}$ are shown in Figure 3-27 and Figure 3-28. It can be seen that the closed-loop system also is better damped at lower speeds and has less damping at higher speeds. A value of d_s = 2.0 m was used for the sensor location.

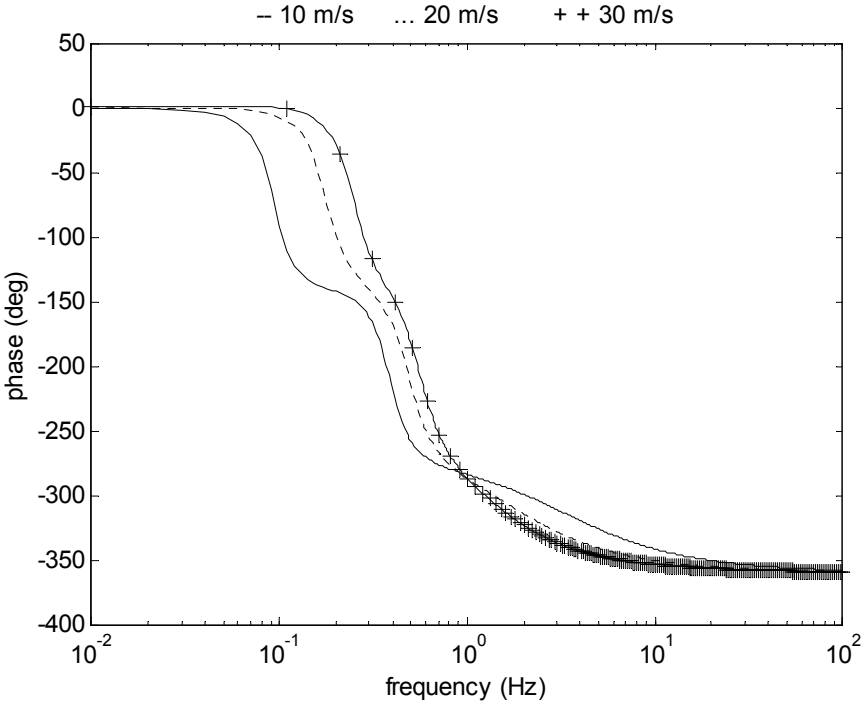

Figure 3-28. Closed-loop transfer function $\dot{\psi} / \dot{\psi}_{des}$ at different speeds (phase)

3.10.2 Performance variation with sensor location

Another important variable that influences closed-loop performance and robustness is the sensor location variable d_s. As seen in Figure 3-29 and Figure 3-30, as the variable d_s is increased, the system is better damped. This is also observed in the time response plots shown in Figure 3-31, where the higher values of d_s gives a better damped step response. A velocity of 30 m/s was used in the simulations.

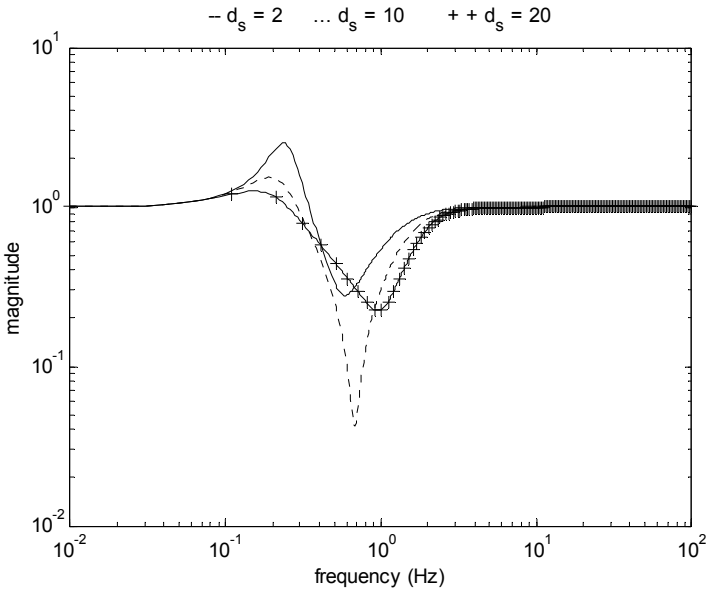

Figure 3-29. Closed-loop transfer function $\dot{\psi} / \dot{\psi}_{des}$ at different values of d_s (magnitude)

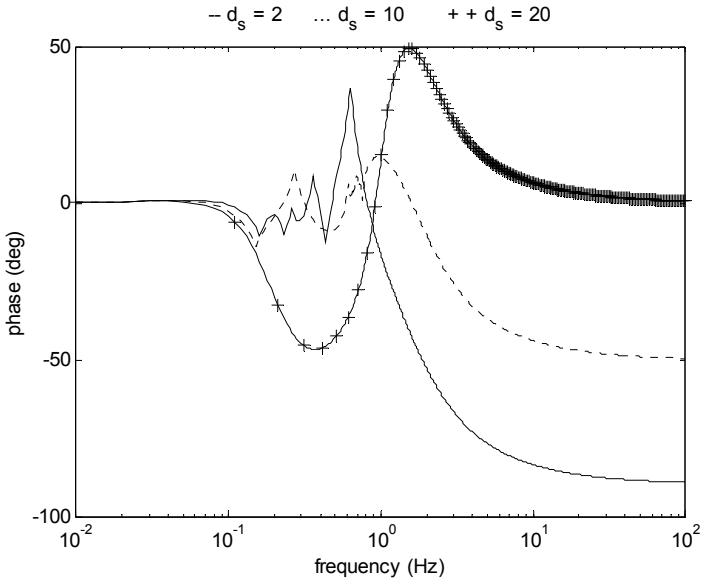

Figure 3-30. Closed-loop transfer function $\dot{\psi} / \dot{\psi}_{des}$ at different values of d_s (phase)

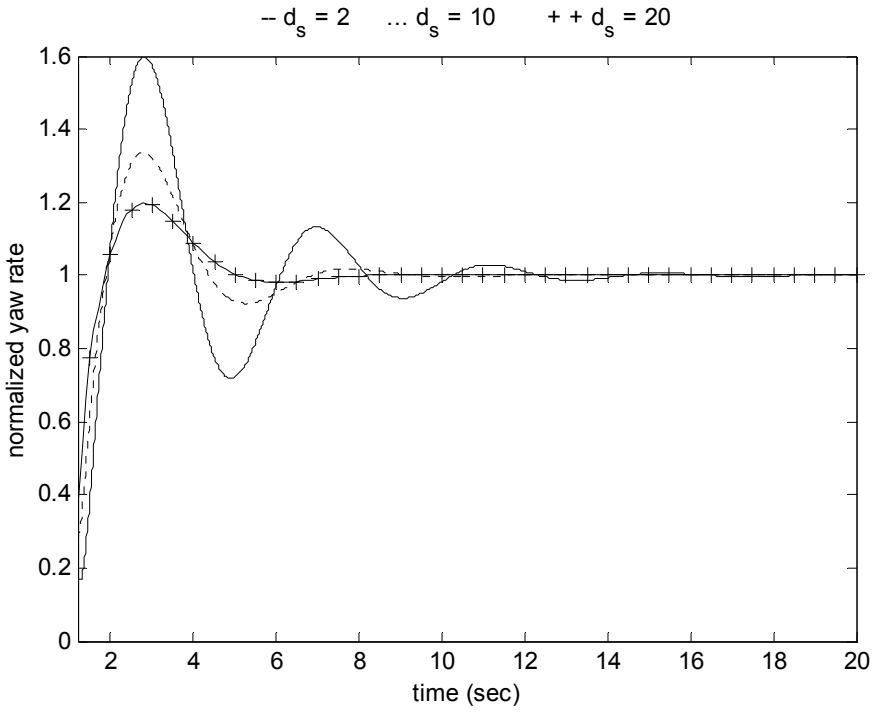

Figure 3-31. Step response of the transfer function $\dot{\psi} / \dot{\psi}_{des}$ at different values of d_s

3.11 COMPENSATOR DESIGN WITH LOOK-AHEAD SENSOR MEASUREMENT

In the previous section, it was seen that larger values of d_s provided better damping in the closed-loop transfer functions. Large values of d_s correspond to "look-ahead" measurement in which the lateral position error with respect to road is measured at a distance significantly ahead of the vehicle. Look ahead measurement is typical when a vision system is used for lateral position measurement. If magnetometers or differential GPS is used for position measurement, then look ahead sensing can be obtained by combining the on-vehicle lateral position measurement with vehicle yaw angle measurement so as to extrapolate the lateral position error to a look-ahead point. In other words, the look ahead distance d_s is artificially increased by measuring both e_1 and e_2 and then calculating $y = e_1 + d_s e_2$, instead of directly measuring $e_1 + d_s e_2$.

The open-loop transfer function $P(s) = \frac{y}{\delta}(s)$ is shown below in the Bode plot in Figure 3-32 for a longitudinal speed of 25 m/s, using $d_s = 15$ meters. From the Bode plot, it can be seen that this look-ahead system has much better phase characteristics than the original system discussed in section 7 which used $d_s = 2$ meters.

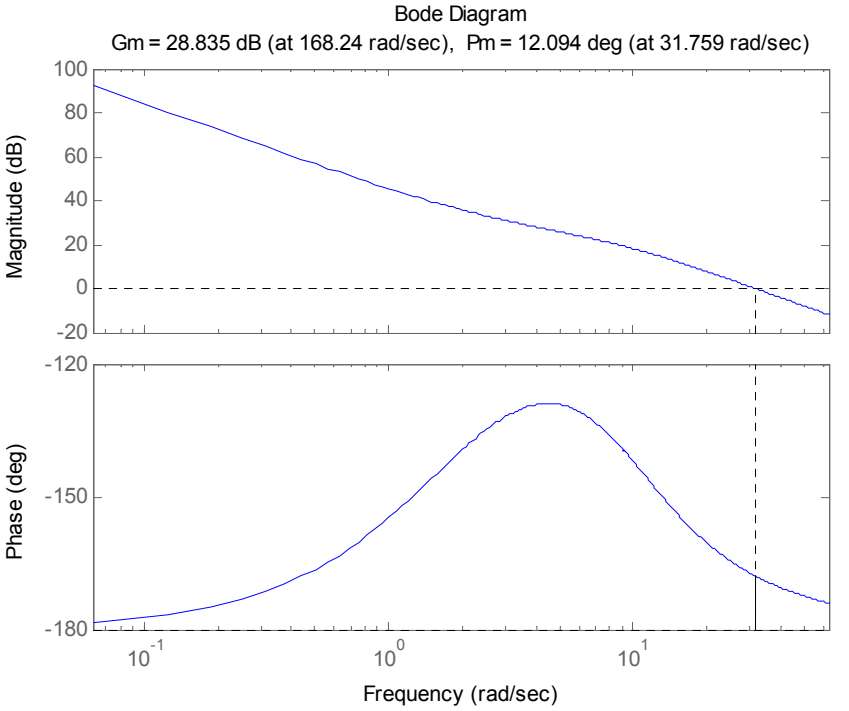

Figure 3-32. Gain & phase margins using proportional feedback with unit gain and a high value of d_s

Adequate phase margin can be obtained for this system simply by reducing the gain at intermediate frequencies appropriately so that crossover occurs at a lower frequency with adequate phase. A lag compensator would be able to adequately perform this task.

3.12 CHAPTER SUMMARY

This chapter discussed steering control system design for lateral lane keeping applications.

First, the use of full information in the form of state feedback was presented. The lateral system is controllable and can be stabilized by state feedback. On a straight road, with the use of a state feedback controller, all position and yaw errors were shown to converge to zero. On a circular road, however, these errors do not converge to zero with state feedback. The use of a feedforward term in the control system enables the position error to converge to zero. However, the yaw angle error will always have a steady state value, resulting in a steady state vehicle slip angle. Equations for the feedforward term and for the steady state slip angle were presented.

Next, control system design using output feedback was discussed. The output measurement was assumed to be lateral position measurement with respect to road center at a look-ahead point. Such a measurement is available from vision cameras and can also be obtained from other types of lateral position measurement systems. Nyquist plots were used to design a control system. It was shown that a proportional controller could stabilize the system if adequately large gains could be used. However, it would still suffer from poor phase margin. The use of a lead compensator together with proportional feedback ensures both adequate phase and gain margins and good performance. Another important result presented in the chapter was that by increasing the look-ahead distance at which lateral position measurement is made, a simple lag compensator would be adequate at providing good performance and robustness.

NOMENCLATURE

e_1	lateral position error with respect to road
e_2	yaw angle error with respect to road
A, B_1, B_2	matrices used in linear state space model for lateral dynamics
δ	steering wheel angle
R	turn radius of vehicle or radius of road
K	feedback gain matrix for state feedback controller
δ_{ff}	feedforward steering angle
δ_{ss}	steady state steering angle
e_{2_ss}	steady state yaw angle error
K_V	understeer gradient

x_{ss}	steady state tracking errors on a curve
F_y	lateral tire force
F_{yf}	lateral tire force on front tires
F_{yr}	lateral tire force on rear tires
V_x	longitudinal velocity at c.g. of vehicle
$\dot{y}$	lateral velocity at c.g. of vehicle
m	total mass of vehicle
I_z	yaw moment of inertia of vehicle
ℓ_f	longitudinal distance from c.g. to front tires
ℓ_r	longitudinal distance from c.g. to rear tires
L	total wheel base ($\ell_f + \ell_r$)
ψ	yaw angle of vehicle in global axes
$\dot{\psi}$	yaw rate of vehicle
X , Y	global axes
α_f	slip angle at front tires
α_r	slip angle at rear tires
C_α	cornering stiffness of tire
F_z	normal force on tire
μ	tire-road friction coefficient
$\dot{\psi}_{des}$	desired yaw rate from road
β	slip angle at vehicle c.g. (center of gravity)
θ_V	velocity angle (angle of velocity vector with longitudinal axis)
θ_{Vf}	velocity angle at front wheels
θ_{Vr}	velocity angle at rear wheels
ϕ	road bank angle
γ	angle subtended by vehicle at center of circular vehicle path

$V_{\min}$ minimum longitudinal velocity

$V_{\max}$ maximum longitudinal velocity

P matrix used in Lyapunov function candidate

d_s look-ahead distance for lateral position measurement

$P(s)$, $C(s)$ plant and controller in unity feedback loop

Γ_s, Γ_{PC} contours used for Nyquist plot

REFERENCES

Ackermann, J. Guldner,J. Sienel,W. Steinhauser, R., Utkin, B.," Linear and nonlinear controller design for robust automatic Steering". *IEEE transactions on Control Systems Technology*, Vol. 3, No. 1, March 1995, pp132-142.

J. Ackermann, "Robust Decoupling, Ideal Steering Dynamics, and Yaw Stabilization of 4WS Cars," *Automatica*, vol. 30, pp. 1761-1768, 1994.

Chen, C. and Tomizuka, M., "Vehicle Lateral Control on Automated Highways: A Back-stepping Approach", *Proceedings of the IEEE Conference on Decision and Control*, December 1997.

Donath, M., Morellas, V., Morris, T. and Alexander, L., "Preview Based Control of a Tractor Trailer Using DGPS for Preventing Road Departure Accidents", *Proceedings of the IEEE Conference on Intelligent Transportation Systems*, ITSC'97, Boston, MA, November, 1997.

Gillespie, T., *Fundamentals of Vehicle Dynamics*, Society of Automotive Engineers, 1992.

Guldner, J., Tan, H.-S. and Patwardhan, S., "Analysis of Automatic Steering Control for Highway Vehicle with Look-Down Lateral Reference Systems", *Vehicle System Dynamics*, vol. 26, no. 4, pp.243-269, 1996.

Guldner, J., Sienel, W., Tan, H.S., Ackermann, J., Patwardhan, S. and Tilman Bunte "Robust automatic steering control for look-down reference systems with front and rear sensors", *IEEE Transactions on Control Systems Technology*, vol.7, No.1, January 1999, pp2-11.

Hingwe, P. and Tomizuka, M., "Experimental evaluation of a chatter free sliding mode control for lateral control in AHS", *Proceeding of the American Control Conference*, Vol. 5, p 3365-3369, 1997. IEEE, Piscataway, NJ, USA, 97CH36041.

Malik, J., "Development of Binocular Stereopsis for Vehicle Lateral Control, Longitudinal Control and Obstacle Detection, "*PATH MOU 257*, Final report.

Patwardhan, S., Tan, H.S and Guldner, J., "A General Framework for Automatic Steering Control: System Analysis," *Proceedings of the American Control Conference*, Vol. 3, pp. 1598-1602, 1997.

Satyajit Patwardhan, Han-Shue Tan, Jurgen Guldner, "Lane Following During Backward Driving for Front Wheel Steered Vehicles", *Proceeding of the American Control Conference*, Albuquerque, New Mexico, June 1997.

Huei Peng and Masayoshi Tomizuka, "Preview Control of Vehicle Lateral Guidance in Highway Automation", *Journal of Dynamic Systems, Measurement, and Control*, Dec.1993, Vol,. 115 P679-685.

Kosecka, J., Blasi, R., Taylor, C.J. and Malik, J., "Vision Based Lateral Control of Vehicles," *Intelligent Transportation Systems*, November 1997, Boston.

R. Rajamani, H.S. Tan, B. Law and W.B. Zhang, "Demonstration of Integrated Lateral and Longitudinal Control for the Operation of Automated Vehicles in Platoons", *IEEE Transactions on Control Systems Technology,* Vol. 8, No. 4, pp. 695-708, July 2000.

R. Rajamani, C. Zhu and L. Alexander, "Lateral Control of a Backward Driven Front Steering Vehicle," *Control Engineering Practice*, to appear, 2003.

Tan, H.S., Guldner, J., Chen, C. and Patwardhan, S., "Lane Changing on Automated Highways with Look Down Reference Systems," *Proceedings of the IFAC Workshop on Advances in Automotive Control*, February 1998.

Taylor, C.J., Kosecka, J., Blasi, R. and Malik, J., "A Comparative Study of Vision-Based Lateral Control Strategies for Autonomous Highway Driving," *International Journal of Robotics Research*, Vol. 18, No. 5, pp. 442-453, May 1999.

Thorpe, C.E., Hebert, M., Kanade, T. and Shafer, S., "Vision and Navigation for the Carnegie-Mellon Navlab, "*IEEE Transactions on Pattern Analysis and Machine Intelligence,* Vol. 10, No. 3, pp. 362-373, May 1998.

Weber, J., Koller, D., Luong, Q.T. and Malik, J., "An Integrated Stereo Based Approach to Automatic Vehicle Guidance, "Proceedings of the International Conference on Computer Vision, Boston, June 1995.

Wong, J.Y., *Theory of Ground Vehicles*, Wiley-Interscience, ISBN 0-471-35461-9, Third Edition, 2001

W.B. Zhang and R.E. Parsons, "An Intelligent Roadway Reference System for Vehicle Lateral Guidance/Control," *Proceedings of the American Control Conference*, San Diego, CA, USA, pp. 281-286, 1990.